

Synthetic Population of Interstellar Objects in the Solar System

Dušan Marčeta^a

^a*Department of Astronomy, Faculty of Mathematics, University of Belgrade, Studentski trg 16, Belgrade, 11000, Serbia*

Abstract

The discovery of the first two macroscopic interstellar objects (ISOs) passing through the Solar System has opened entirely new perspectives in planetary science. The exploration of these objects offers a qualitatively new insight into the processes related to the origin, structure and evolution of planetary systems throughout the Galaxy. Knowledge about these phenomena will greatly advance if current and future sky surveys discover more ISOs. On the other hand, the surveys require better characterization of this population in order to improve their discovery algorithms. However, despite their scientific significance, there is still no comprehensive orbital model of ISOs in the Solar System and computationally efficient algorithm for generating their synthetic representations that would respond to these increasing needs. Currently available method for generating synthetic populations cannot fully take into account important phenomena, such as gravitational focusing and the shielding effect of the Sun. On the other hand, this method is also computationally far too demanding to be used for systematic exploration of the ISO population. This paper presents an analytical method for determining the distributions of the orbital elements of ISOs, as well as computationally efficient algorithm for generating their synthetic populations, based on the multivariate inverse transform sampling method. The developed method is several orders of magnitudes more efficient than the available method, depending on the size of the synthetic population. A Python implementation of the method is freely available and can be used to generate synthetic populations of ISOs with user-defined input parameters.

Keywords: Planetary systems, comets: general, minor planets, asteroids: general, minor planets, asteroids: individual: 1I/'Oumuamua, comets: individual: 2I/Borisov

1. Introduction

After the discovery of the first two interstellar visitors, 'Oumuamua (Williams, 2017) and Borisov (Borisov, 2019) the population of interstellar objects (ISOs) has come into the focus of planetary science and other fields of astronomy and astrophysics. These objects could provide an in-depth insight into the formation, structure and various stages of evolution of planetary systems (Trilling et al., 2017a), and may even be the seeds for the formation of planets (Pfalzner and Bannister, 2019; Moro-Martín and Norman, 2022). Their composition, size, shape and rotational state may be linked to the mechanisms responsible for their ejections in the interstellar space (Jackson et al., 2018; Ćuk, 2018; Pfalzner et al., 2021; Childs and Martin, 2022), thus offering a unique validation of the models of formation and evolution of the planetary systems. Measurements of production rates of CO₂, CO and H₂O of future interstellar comets can provide constraints on their primordial C/O ratios, which can be used as an indicator for their formation location within a protostellar disk. In this way, interstellar comets offer a key insight into mechanisms responsible for cometary ejection in exoplanetary systems (Seligman et al., 2022). ISOs could also be laboratories for examination of the interstellar environment which they passed through, the impact of this environment on their sizes, shapes and rotational states (Vavilov and Medvedev, 2019; Zhou, 2020; Phan et al., 2021), and galactic weathering processes (Jewitt et al., 2017; Fitzsimmons et al., 2018). Finally, they could even offer an exclusive opportunity for in situ explo-

ration of these distant worlds, thereby presenting a realistic alternative to the interstellar and cross galactic voyage (Snodgrass and Jones, 2019; Moore et al., 2021; Seligman and Laughlin, 2018). A comprehensive review on the ISO population can be found in Jewitt and Seligman (2022).

There are many studies that are directly related to the orbital structure of interstellar objects in the Solar System and around other stars, which could benefit from a realistic model of this population and efficient algorithm for generating its synthetic representations. Such a model can be very useful for developing algorithms for determining their orbits (e.g. Gronchi et al., 2021) and analysing their detection rates (Marčeta and Novaković, 2020; Hoover et al., 2022) by the future sky surveys. On the other hand, it is also related to the exploration of dynamical mechanisms for their permanent capture by the planetary systems (Dehnen and Hands, 2021) and the Solar System in particular (Napier et al., 2021a,b). ISOs could not only be temporary visitors, but also permanent residents of the Solar System with possible ~8 'Oumuamua analogues inside Jupiter's orbit at any time (Dehnen et al., 2021). Moreover, some particular main belt asteroids and Centaurs may be associated with an interstellar origin (Namouni and Morais, 2020). However, Morbidelli et al. (2020) identify that the Halley-type comets and the Oort cloud are the most likely sources of retrograde co-orbitals and highly inclined Centaurs.

Numerous models of other Solar System populations have been developed for different purposes. Most refer to the NEO population (Greenstreet et al., 2012; Granvik et al., 2018), but

there are also models of other populations, such as Main Belt population (Tedesco et al., 2005), comets in the outer Solar System (Silsbee and Tremaine, 2016), and a comprehensive model of the Solar System which is used to analyse the performance of Pan-STARRS survey and which includes all major populations (Grav et al., 2011).

However, despite the high importance of the ISO population, there is still no comprehensive orbital model nor computationally efficient algorithm for generating synthetic representations of this population in the Solar System. The objective of the study presented in this paper is to define the distribution functions of all orbital elements of ISOs in arbitrary volume of space around the Sun, and to develop a procedure for sampling orbits from these distributions, which is computationally efficient enough to enable its systematic application. The synthetic population of ISOs is generated under the assumption that its kinematic distribution is the same as that of stars in the solar neighborhood, as a consequence of dynamical relaxation through the scattering events of giant molecular clouds and dark matter substructure (Seligman and Laughlin, 2018; Hoover et al., 2022). This kinematics is described by the Schwarzschild velocity ellipsoid with respect to the Local Standard of Rest (LSR), with velocity dispersions σ_1 , σ_2 , σ_3 and the vertex deviation v_d defining the orientation of the ellipsoid with respect to the Galactic reference frame.

This paper is organised as follows. Section 2 qualitatively and quantitatively analyzes the effect of gravitational focusing. Section 3 describes the currently available methods for generating synthetic population of ISOs along with their limitations and shortcomings. The initial version of this method does not take into account the effect of gravitational focusing outside the sphere in which the synthetic population is generated. Since this method is based on the propagation of the equation of motion, i.e. hyperbolic Kepler equation, it will hereafter be referred to as the *Dynamical method (without focusing)*. Subsection 3.1 describes a modification of this method in order to take into account the effect of gravitational focusing outside the sphere in which the synthetic population is generated. This modification will hereafter be referred to as *Dynamical method (with focusing)*. Section 4 describes a newly developed method to overcome the drawbacks of the existing methods. Since this method is based on the sampling from the probability distributions of the orbital elements, it will be hereafter referred to as the *Probabilistic method*. Section 5 summarizes the results of the study and it is divided into three subsections: Subsection 5.1 which compares synthetic populations of ISOs with different distributions of interstellar velocities, Subsection 5.2 which analyzes accuracy and computational efficiency of the newly developed method and its comparison with the existing ones, and Subsection 5.3 which evaluates limitations of the developed method. Section 6 summarises the most important conclusions of the work.

2. The effect of gravitational focusing

Considered homogeneous in interstellar space, a structure of the ISO population in the Solar System is disturbed by the

influence of the Sun's gravity, and to significantly lesser extent by the gravity of the other Solar System objects. As shown later, planets can significantly affect the orbits of individual objects, but they cannot disturb the structure of the ISO population. Therefore, when generating synthetic population of ISOs using the *Probabilistic method*, only the gravity of the Sun is taken into account.

Semi-major axis (a), eccentricity (e) and perihelion distance (q) of an ISO are defined by its interstellar velocity (v_∞) and impact parameter (B) (e.g. Kemble, 2006).

$$\begin{aligned} a &= -\frac{\mu}{v_\infty^2} \\ q &= a + \sqrt{a^2 + B^2}, \\ e &= \sqrt{1 + \frac{B^2}{a^2}} \end{aligned} \quad (1)$$

where μ is the standard gravitational parameter of the Sun.

The interstellar velocity v_∞ is defined as the magnitude of the heliocentric velocity vector when the object is at a very large heliocentric distance, so that the effect of the Sun's gravity can be neglected (the so-called hyperbolic excess velocity). On the other hand, the impact parameter B is the distance of this velocity vector from the Sun (see Figs. 1 and 2).

In a qualitative sense, the effect of gravitational focusing works as follows. The Sun's gravity curves the orbits of slower objects more than the orbits of faster ones. According to Eqs. 1, an object with a lower interstellar velocity (energy) also has a smaller semi-major axis (larger by absolute value). Accordingly, this object has a smaller perihelion distance and eccentricity for the same impact parameter. This means that a decrease in interstellar velocity increases the effective cross-section that objects have to traverse at infinity in order to reach a certain heliocentric distance. The situation is similar with the impact parameters. For the same interstellar velocity, an object with smaller B has smaller q and e compared to an object with larger B . Schematic illustration of this effect is shown in Fig. 1.

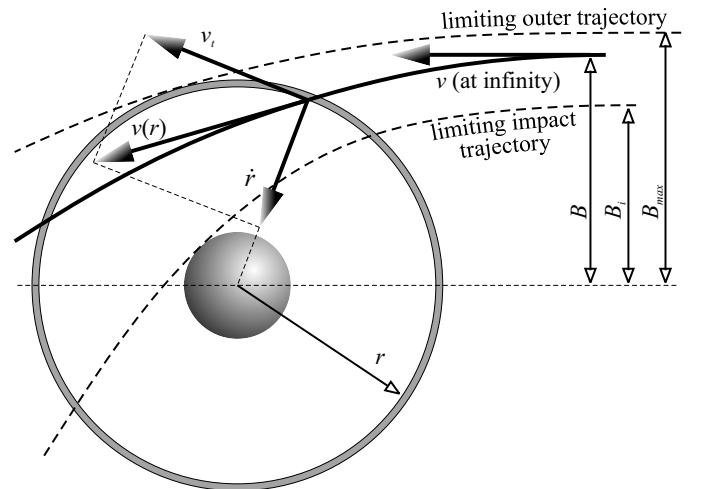


Figure 1: Schematic illustration of incoming trajectory of an ISO crossing an infinitesimal heliocentric spherical shell and characteristic boundary trajectories.

As a consequence of this effect, through a heliocentric spherical shell of arbitrary radius r pass objects whose impact parameters are smaller than or equal to r (as it would be the case without the effect of gravitational focusing), but also objects with larger impact parameters whose orbits are bent enough to reach heliocentric distance r . The maximum impact parameter that allows an object to reach an arbitrary heliocentric distance can be easily determined from the conservation of energy and angular momentum,

$$\frac{1}{2} (v_t^2 + v_r^2) - \frac{\mu}{r} = \frac{1}{2} v_\infty^2, \quad (2)$$

$$r \cdot v_t = B \cdot v_\infty,$$

where v_t is tangential and v_r is radial component of an ISO's velocity vector at arbitrary heliocentric distance r .

The expression for radial velocity at an arbitrary heliocentric distance r can be derived from Eqs. 2,

$$v_r = \frac{1}{r} \sqrt{v_\infty^2 r^2 + 2\mu r - B^2 v_\infty^2}. \quad (3)$$

For a given v_∞ , the limiting impact parameters B_1 and B_2 (see Fig. 1) can be determined from Eq. 3 by setting $v_r = 0$ for the bounding outer trajectory, and $r = R$ (R is solar radius) for the bounding impact trajectory, giving

$$B_1 = R \sqrt{1 + \frac{2\mu}{v^2 R}}, \quad (4)$$

$$B_2 = r \sqrt{1 + \frac{2\mu}{v^2 r}}.$$

From the expression for the maximum impact parameter in Eq. 4, a ratio between effective and geometrical cross-sections can be obtained in the form

$$\left(\frac{B_2}{r}\right)^2 = 1 + \frac{v_{esc}^2}{v^2}, \quad (5)$$

where $v_{esc} = \sqrt{2\mu/r}$ is the escape velocity at heliocentric distance r . As already pointed out, Eq. 5 shows that the effective cross-section, which any object has to pass at infinity in order to reach heliocentric distance r , increases if the interstellar velocity decreases. This means that at any heliocentric distance, the increase in number-density will be greater for slower objects in the population because these objects have larger effective cross-sections, and thus can reach that heliocentric distance from a larger volume of space compared to faster objects. According to Eq. 5, if the heliocentric distance decreases, the ratio between the effective and geometric cross-section increases, which is why the effect of gravitational focusing is more pronounced at small heliocentric distances. However, due to the physical dimensions of the Sun, at some point, a so-called shielding effect of the Sun becomes dominant over the effect of gravitational focusing, which leads to a decrease in number-density of the population with a further decrease in heliocentric distance. This effect will be elaborated in more detail later.

It follows from the above analysis that the gravity of the Sun affects the ISO population by increasing their number-density

relative to interstellar space. This increase depends on heliocentric distance and interstellar velocities of ISOs. The resulting influence on the distributions of the orbital elements of ISOs around the Sun is the most important problem to be solved in order to generate their synthetic population.

3. Dynamical method for generating synthetic population of ISOs

Previous analyzes involving synthetic populations of ISOs (e.g. Engelhardt et al., 2017; Marčeta and Novaković, 2020) used a technique developed by Grav et al. (2011). This technique is based on propagating an initially homogeneous and isotropic population over a sufficiently long time so that the resulting population represents a steady-state population altered by the effect of gravitational focusing in some predefined sphere surrounding the Sun. To resolve the effect of gravitational focusing on the initially homogeneous population, this method consists of the following steps:

1. Defining a sphere around the Sun where the ISO population will be generated. This sphere is called the *model sphere*. It is assumed that the population is initially homogeneous in this sphere and its kinematics follow a distribution assumed to represent realistic kinematics of ISOs in interstellar space.
2. Calculating the time required for this sphere to be completely emptied of all initial objects. This time is called the *initialization time*. This ensures that, at the end of the propagation, this sphere is completely populated by objects that were initially outside this sphere, where the gravitational focusing is considered to be negligible, so the assumed homogeneous population is very similar to the real population of ISOs.
3. Calculating the maximum heliocentric distance from which the fastest object from the population can reach the *model sphere* during the *initialization time*. A sphere with this radius is called the *initialization sphere*. Objects outside this sphere cannot reach the *model sphere* during the *initialization time*, so these objects are not taken into account.
4. The initial population is generated inside the *initialization sphere* and propagated for the *initialization time* by solving the hyperbolic Kepler equation. All objects located inside the *model sphere* at the end of the *initialization time* make up the synthetic population of ISOs inside this sphere.

This procedure results in the *model sphere* being populated only with objects that were initially outside this sphere, where it is assumed that the gravitational focusing is negligibly small. Although this procedure allows the generation of ISO population that is very similar to the real population, it still has two major drawbacks. The first is that it requires setting a certain heliocentric distance beyond which the gravitational focusing can be completely neglected. As discussed earlier, Eq. 5 which can be considered a simple quantification of the gravitational focusing shows that this effect is stronger for slower objects than for faster ones. This means that setting any heliocentric

distance beyond which this effect is neglected will lead to a certain underestimation of slower objects in the final synthetic population. Although this underestimation is small, it may be significant because slower objects may more likely be discovered by the sky surveys or captured in the Solar System by some of the dynamical mechanisms (Napier et al., 2021a; Dehnen et al., 2021).

The other drawback of this procedure is that it is very computationally demanding. To illustrate the magnitude of the computational load required by this method, a brief analysis is given for the generation of population inside the *model sphere* with radius of 100 *au* and with a range of initial velocities between 1 *km/s* and 100 *km/s*. The minimum velocity defines the *initialization time*, required for all objects to leave the *model sphere*, which in this case is about 205 years. This time, together with the maximum predefined velocity, defines the radius of the *initialization sphere*, which in this case is about 4500 *au*. This results in an enormous initialization volume of about 382 billion *au*³. This volume is almost 5 orders of magnitude larger than the volume of the *model sphere*, resulting in a similar ratio of the numbers of initial objects and final objects that make up the synthetic population of ISOs. Number-density of ISOs is very unconstrained, with estimations ranging from 10^{-9} au^{-3} ($\sim 10^7 \text{ pc}^{-3}$) (Moro-Martín et al., 2009) to $\sim 10^{-1} \text{ au}^{-3}$ ($\sim 10^{15} \text{ pc}^{-3}$) (Laughlin and Batygin, 2017; Trilling et al., 2017b; Jewitt et al., 2017; Do et al., 2018; Levine et al., 2021). However, even for the most conservative assumptions about number-density and reasonable size-frequency distributions, it is quite easy to achieve number-density of 1 object per *au*³ for 10 meter-sized objects already, which could for instance be detected by the Vera Rubin Observatory’s Legacy Survey of Space and Time (Schwamb et al., 2021). This results in a very large number of objects whose states have to be determined at the beginning and end of the *initialization time* in order to select those which are within the *model sphere* at that moment. This procedure requires about 2000 hours on 6-Core 3.0GHz CPU. Increasing the range of initial velocities, size of the model sphere and/or number-density results in a further increase in computational load.

3.1. Modification of the Dynamical method

The described procedure ignores gravitational focusing outside the model sphere. If the *model sphere* is small, this leads to significant underestimation of the number of objects in the resulting population, especially in the lower part of the velocity distribution. To overcome this problem, the initial population outside the model sphere can be modified according to the method applied in Seligman and Laughlin (2018) and Hoover et al. (2022). The *initialization sphere* is divided into spherical shells, and the velocity distribution is divided into narrow bands. For each band $\Delta v = (\Delta v_1, \Delta v_2, \Delta v_3)$, the spatial number-density of ISOs is given by

$$n(\Delta v) = \frac{n}{8} \prod_{i=1}^3 \operatorname{erf} \left(\frac{v_i}{\sqrt{2}\sigma_i} \right) \Big|_{v_i - \Delta v_i}^{v_i + \Delta v_i}. \quad (6)$$

The increase in number-density for objects falling within these velocity ranges is calculated in each spherical shell according to

$$\xi = \sqrt{1 + \left(\frac{v_{esc}}{v_\infty} \right)^2}. \quad (7)$$

where $v_{esc} = \sqrt{2\mu/r}$ is the solar escape velocity in the middle of each spherical shell. After the initial positions of ISOs are generated, to account for the solar acceleration, each velocity vector is multiplied by a factor $\sqrt{v_\infty^2 + v_{esc}^2}/v_\infty$.

This modification makes it possible to largely overcome one of the main drawbacks of the previously described procedure, but its result still deviates slightly from the real population. Although it adjusts the speed of objects located at arbitrary heliocentric distances due to the solar acceleration, the directions of the velocity vectors are assumed to be the same as at infinity. Since solar acceleration also bends the orbits of ISOs, the velocity vectors at an arbitrary heliocentric distance point closer to the Sun compared to the corresponding interstellar velocity vectors. Neglecting this the objects are given a slightly larger angular momentum, and this results in a comparably larger eccentricity and perihelion distance. This effect is very small and noticeable only for very small model spheres, as shown in section 5.2.

4. Probabilistic method for generating synthetic population of the ISOs

A completely different approach can be applied in order to overcome the limitations of the *Dynamical methods*. The idea is to derive probability functions of the orbital elements of ISOs and to use them to directly sample their orbits using the inverse transform sampling method (e.g. Devroye, 1986). This approach has two advantages over the *Dynamical methods*. Firstly, it allows the treatment of the effect of gravitational focusing without the restriction used in the *Dynamical methods*. Secondly, it allows direct sampling of orbits only for the objects that make up the synthetic population, without the need to treat an enormous number of initial objects of which only a tiny part makes the final population, as is the case with the *Dynamical methods*. For the sake of notation, boldface symbols with subscript *s* denote generated sets of the orbital elements (e.g. \mathbf{q}_s denotes the set of perihelion distances), while the same regular type face symbols denote arbitrary elements from the corresponding set (e.g. q_s denotes an arbitrary element from the set of perihelion distances \mathbf{q}_s).

4.1. Deriving probability distribution of orbital parameters of ISOs

Early works by Beard (1959) and Hale and Wright (1964) analysed the increased concentration of interplanetary meteoroids compared to interplanetary space due to gravitational focusing by the Earth. Colombo et al. (1966) and Singer (1961) derived analytical expressions to describe the increased flux of the interplanetary meteoroids at arbitrary geocentric distance. These expressions can be used as a basis for deriving the probability density function of the orbital elements of ISOs in the Solar System. The geometrical constellation of an ISO approaching the Sun from infinity is illustrated in Fig. 2.

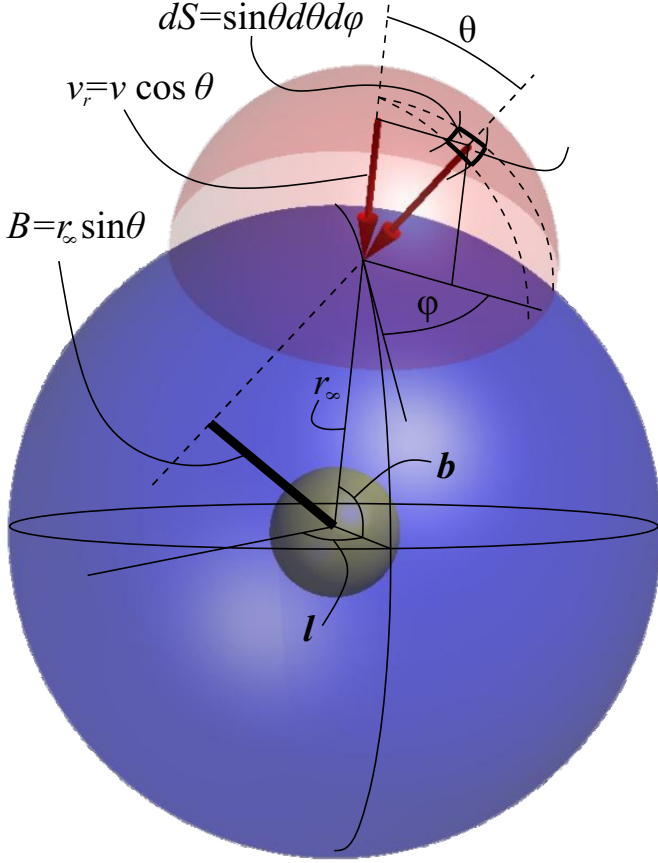


Figure 2: Geometrical constellation of an ISO approaching the Sun from infinity.

The total number of objects per unit time that enter a sphere of radius r_∞ around the Sun is

$$F = 4\pi r_\infty^2 \int_{v_\infty(\min)}^{v_\infty(\max)} \int_0^{2\pi} \int_{-\frac{\pi}{2}}^{\frac{\pi}{2}} \int_0^{\frac{\pi}{2}} \int_0^{2\pi} n v_\infty \cos \theta \sin \theta d v_\infty dl db d\theta d\varphi, \quad (8)$$

where n is the total interstellar number-density of objects, which generally, for anisotropic population, depends on interstellar velocity vector defined by v_∞ , l , b , θ and φ , where l and b are galactic longitude and latitude, respectively, and angles θ and φ are defined in Fig. 2.

When radius r_∞ approaches infinity, velocity vector becomes hyperbolic excess velocity vector and the impact parameter B can be defined as $B = r_\infty \sin \theta$, (see. Fig. 2). On the other hand, angle θ approaches zero for all objects that can reach an arbitrary heliocentric distance. Consequently, at infinity, number-density of objects capable of reaching arbitrary heliocentric distance is not a function of θ and φ , but only of v_∞ , l and b . Integrating with respect to θ and φ leads to

$$n_{v_\infty, l, b} = 4\pi n_0 p_{v_\infty, l, b}, \quad (9)$$

where n_0 is the total interstellar number-density, and $p_{v_\infty, l, b}$ is the distribution of ISOs with respect to magnitude and direction

of interstellar velocity vector. Now Eq. 8 can be reformulated into

$$F = n_0 \int_{v_\infty(\min)}^{v_\infty(\max)} \int_0^\infty \int_0^{2\pi} \int_{-\frac{\pi}{2}}^{\frac{\pi}{2}} \int_0^{2\pi} p_{v_\infty, l, b} v_\infty B d v_\infty dB dl db d\varphi. \quad (10)$$

Eq. 10 presents the total (integral) flux of ISOs. Differentiation of Eq. 10 with respect to v_∞ , B , l , b and φ , gives the differential flux that depends on these five variables, in the form

$$F_{v_\infty, B, l, b, \varphi} = n_0 p_{v_\infty, l, b} v_\infty B. \quad (11)$$

As one can see, this function does not depend on φ . This means that this angle can be drawn from a uniform distribution from $(0, 2\pi)$, as it was done in Seligman and Laughlin (2018) and Hoover et al. (2022).

Out of all objects coming from infinity, only a fraction will penetrate deep enough to enter a sphere of arbitrary radius r . Depending on their v_∞ and B , some of these objects will cross an infinitesimally thin shell of radius r twice, and some of these objects will impact the Sun, so they will do that only once (see Fig. 1). With this in mind, at an arbitrary heliocentric distance r , the former objects will contribute to number-density twice as large as the latter ones.

Due to conservation of the particles, the total number-density of objects in a spherical shell with arbitrary radius r (i.e. with heliocentric distances between r and $r + dr$), with interstellar velocities between v_∞ and $v_\infty + dv_\infty$, impact parameters between B and $B + dB$, velocity direction angle between φ and $\varphi + d\varphi$, coming from the part of the sky bounded by l , $l + dl$, b and $b + db$, can be obtained by dividing the flux defined by Eq. 11 by the area of the shell ($4r^2\pi$) and radial velocity of objects defined by Eq. 3, giving

$$n_{r, v_\infty, B, l, b, \varphi} = n_0 p_{r, v_\infty, B, l, b, \varphi} = n_0 p_6 = \begin{cases} n_0 \frac{v_\infty p_{v_\infty, l, b}}{4\pi r} \frac{B}{\sqrt{v_\infty^2 r^2 + 2\mu r - B^2 v_\infty^2}}, & B \leq B_1 \\ n_0 \frac{v_\infty p_{v_\infty, l, b}}{2\pi r} \frac{B}{\sqrt{v_\infty^2 r^2 + 2\mu r - B^2 v_\infty^2}}, & B_1 < B \leq B_2 \end{cases}, \quad (12)$$

where B_1 and B_2 are the critical impact parameters defined by Eq. 4 and illustrated in Fig. 1. Function $p_{r, v_\infty, B, l, b, \varphi}$, defined in Eq. 12 is a joint probability density functions of 6 parameters which uniquely define orbits of ISOs. This function will be used to sample their orbits in arbitrary volume of space around the Sun and for arbitrary distribution of their interstellar velocity vectors. To simplify notation, this function will hereafter be referred to as p_6 .

As mentioned earlier, kinematics of ISOs in interstellar space can be described by the Schwarzschild distribution. To transform Schwarzschild velocity ellipsoid in the Galactic (U, V, W)

Stellar type	σ_R	σ_ϕ	σ_Z	Vertex deviation ($^\circ$)
M	31	23	16	7
G	26	18	15	12
O/B	12	11	9	36

Table 1: Parameters in the Schwarzschild Distributions for Different Stellar Types.

system to spherical (v_∞, l, b) system, it is multiplied by the Jacobian of the transformation,

$$p_{v_\infty, l, b} = f(U, V, W) \begin{vmatrix} \frac{\partial U}{\partial v_\infty} & \frac{\partial U}{\partial l} & \frac{\partial U}{\partial b} \\ \frac{\partial V}{\partial v_\infty} & \frac{\partial V}{\partial l} & \frac{\partial V}{\partial b} \\ \frac{\partial W}{\partial v_\infty} & \frac{\partial W}{\partial l} & \frac{\partial W}{\partial b} \end{vmatrix}. \quad (13)$$

Taking into account that

$$\begin{bmatrix} U \\ V \\ W \end{bmatrix} = \begin{bmatrix} v_\infty \cos b \cos l \\ v_\infty \cos b \sin l \\ v_\infty \sin b \end{bmatrix}, \quad (14)$$

Eq. 13 becomes

$$p_{v_\infty, l, b} = f(U, V, W) v_\infty^2 \cos b. \quad (15)$$

For the purpose of demonstrating the *Probabilistic method*, three different Schwarzschild distributions were used. Parameters of these distributions with respect to the LSR are given in Table 1 (Seligman and Laughlin, 2018; Hoover et al., 2022; Binney and Michael, 1998). Solar motion with respect to the LSR is defined by the velocity components - $U_\odot = 10$ km/s, $V_\odot = 11$ km/s, $W_\odot = 7$ km/s (Bland-Hawthorn and Gerhard, 2016). However, the *Probabilistic method* can be equally applied to any other distribution of interstellar velocities.

4.2. Generating samples of orbital parameters of ISOs

As mentioned earlier, parameters r, v_∞, B, l, b and φ uniquely define orbits of ISOs. This makes function p_6 (Eq. 12) sufficient to generate a synthetic population of ISOs in arbitrary volume of space around the Sun. According to the multivariate inverse transform sampling method, which is used for generating synthetic orbits of ISOs, a parameter is sampled by inverting a joint probability function which is cumulative with respect to that parameter, conditional with respect to parameters already determined, and marginal with respect to parameters yet to be determined. In order to distinguish the four types of probability functions that appear during the application of this method, a special notation is used. The joint probability density function of some parameters is denoted by putting those parameters in the subscript (e.g. $p_{r, v_\infty, B, l, b, \varphi}$ is a joint probability density function of r, v_∞, B, l, b and φ). The distribution

function that is cumulative with respect to some parameter is denoted by adding *cdf* to that parameter in the function name (e.g. $p_{r, v_\infty, B, cdf, l, b, \varphi, cdf}$ is a probability density function with respect to r, v_∞, l and b , but cumulative with respect to B and φ). In the case of a marginal probability function with respect to some parameter, that parameter is omitted from the subscript in the function name (e.g. p_{r, v_∞} is the probability density function with respect to r and v_∞ that is marginal with respect to all other parameters, which means that it includes objects with all possible values of these parameters). Finally, when the distribution is conditional with respect to some parameters, those parameters are put in the brackets (e.g. $p_{v_\infty, cdf}(r_0, B_0)$ is a function which is cumulative with respect to v_∞ , corresponds to some specific heliocentric distance r_0 and impact parameter B_0 , and marginal with respect to other parameters).

The resulting generated sample is independent of the sampling order of the parameters. However, to sample ISO orbits in an arbitrary sphere around the Sun, the total number of objects in that sphere must first be determined. The integration of function $n_{r, v, \varphi, B, l, b}$ (Eq. 12) over the whole domain of all parameters except r gives the variation of number-density of ISOs with heliocentric distance, defined by

$$n_r = n_0 p_r = n_0 \int_{v_\infty(\min)}^{v_\infty(\max)} \int_0^{B_2} \int_0^{2\pi} \int_{-\frac{\pi}{2}}^{\frac{\pi}{2}} \int_0^{2\pi} p_6 dv_\infty dB dl db d\varphi. \quad (16)$$

Function p_6 (Eq. 12) can be integrated analytically with respect to φ and B , giving

$$p_{r, B, cdf, \varphi, cdf} = \begin{cases} \frac{\varphi}{4\pi} \int_{v_\infty(\min)}^{v_\infty(\max)} \int_0^{2\pi} \int_{-\frac{\pi}{2}}^{\frac{\pi}{2}} p_{v_\infty, l, b} \left(\sqrt{1 + \frac{2\mu}{rv_\infty^2}} - \sqrt{1 + \frac{2\mu}{rv_\infty^2} - \frac{B^2}{r^2}} \right) dv_\infty dl db, & B \leq B_1 \\ \frac{\varphi}{4\pi} \int_{v_\infty(\min)}^{v_\infty(\max)} \int_0^{2\pi} \int_{-\frac{\pi}{2}}^{\frac{\pi}{2}} p_{v_\infty, l, b} \left(\sqrt{1 + \frac{2\mu}{rv_\infty^2}} + \sqrt{1 + \frac{2\mu}{rv_\infty^2} - \left(\frac{R}{r}\right)^2 \left(1 + \frac{2\mu}{v_\infty^2 R}\right)} - 2 \sqrt{1 + \frac{2\mu}{rv_\infty^2} - \frac{B^2}{r^2}} \right) dv_\infty dl db, & B_1 < B \leq B_2 \end{cases} \quad (17)$$

As stated above, this is a probability density function of r that is cumulative with respect to B and φ and marginal with respect to v_∞, l and b (i.e. integrated over the whole domain).

In marginal cases also for B and φ , when $B = B_1$ (for impactors) or $B = B_2$ (for both impactors and passers) and $\varphi = 2\pi$, function $p_{r,Bcdf,\varphi cdf}$ becomes marginal with respect to all parameters, except r , in the form

$$p_r = \left\{ \begin{array}{l} \int_{v_{\infty(\min)}}^{v_{\infty(\max)}} \int_0^{2\pi} \int_{-\frac{\pi}{2}}^{\frac{\pi}{2}} \frac{p_{v_{\infty},l,b}}{2} \left(\sqrt{1 + \frac{2\mu}{rv_{\infty}^2}} - \sqrt{1 + \frac{2\mu}{rv_{\infty}^2} - \left(\frac{R}{r}\right)^2 \left(1 + \frac{2\mu}{v_{\infty}^2 R}\right)} \right) dv_{\infty} dl db, \quad B = B_1 \\ \int_{v_{\infty(\min)}}^{v_{\infty(\max)}} \int_0^{2\pi} \int_{-\frac{\pi}{2}}^{\frac{\pi}{2}} \frac{p_{v_{\infty},l,b}}{2} \left(\sqrt{1 + \frac{2\mu}{rv_{\infty}^2}} + \sqrt{1 + \frac{2\mu}{rv_{\infty}^2} - \left(\frac{R}{r}\right)^2 \left(1 + \frac{2\mu}{v_{\infty}^2 R}\right)} \right) dv_{\infty} dl db, \quad B = B_2 \end{array} \right. \quad (18)$$

Integration in Eq. 18 with respect to v_{∞} , l and b is conducted numerically to obtain variation of number-density with heliocentric distance. All results presented in this paper were obtained by applying Simpson's integration rule with steps $\Delta r = 0.1$ au, $\Delta v = 1$ km/s, $\Delta l = \Delta b = 1^\circ$. The variations of number-density with heliocentric distance for the three velocity distributions defined in Table 1 are shown in Figure 3.

Objects that approach very close to the Sun may perish before the perihelion passage due to disintegration, outgassing torques, tidal disruption, etc. In order to survive, they must satisfy the so-called *perihelion survival limit* Bortle (1991). Observational constraints on the behavior of sungrazing comets near perihelion come mostly from the well known Kreutz group. These objects do not survive perihelion. Their brightness usually peaks at 10–15 solar radii and then rapidly fade (Knight and Walsh, 2013). In the context of the *Probabilistic method*, these objects should be viewed as solar impactors because they contribute to the population only on the inbound branches of their orbits. In this sense, the radius R in Eqs. 4, 17 and 18 should be considered as the effective radius that protects the space behind from incoming objects. Obviously, this radius depends on the physical characteristics of the object, its rotational state, etc, and it can be defined as input parameter in the *Probabilistic method*. This effect does not change the character of the curves shown in the bottom panel of Fig. 3, but shifts them to greater heliocentric distances.

The total number of objects inside an infinitesimal spherical shell with an arbitrary radius r is

$$N_{dr} = 4\pi r^2 p_r n_0 dr. \quad (19)$$

The total number of objects inside a heliocentric sphere with radius r is obtained by integrating N_{dr} with respect to r ,

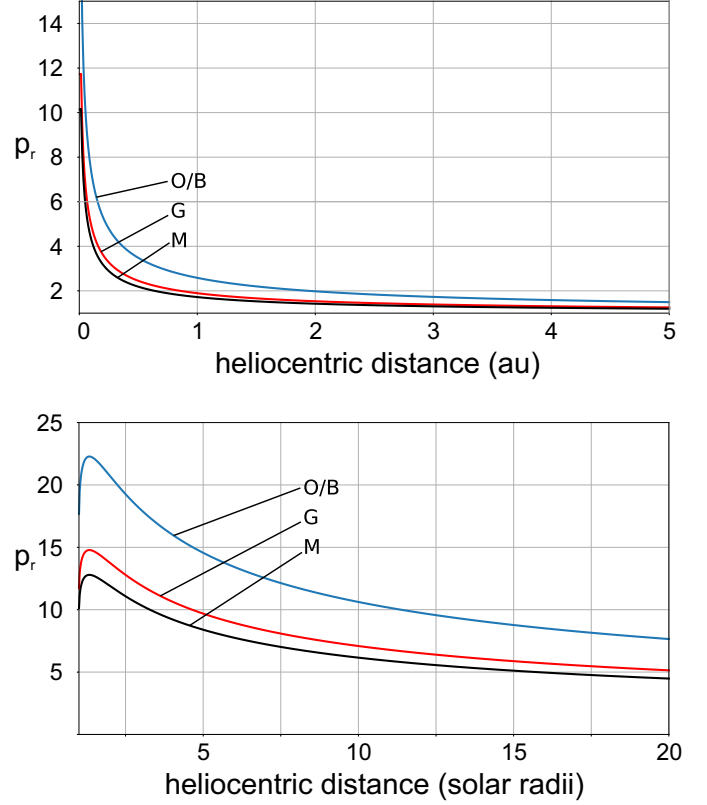


Figure 3: Variation of number-density of ISOs with the heliocentric distance, assuming kinematics of stellar classes M, G and O/B (see Table 1). The top panel shows this variation over the larger range of heliocentric distances that traverse the planetary orbits. The bottom panel shows this variation at small heliocentric distances comparable to the solar radius.

$$N_r = 4\pi n_0 \int_R^r p_r r^2 dr, \quad (20)$$

where R is the effective radius of the Sun.

The 6-step procedure for sampling the 6 parameters used to determine orbital elements of ISOs works as follows.

Step 1

Function N_r allows sampling of heliocentric distances of ISOs using the inverse transform sampling method. As schematically illustrated in Fig. 4, a uniform sample $\mathbf{u}_r = U(0, \max(N_r))$ is transformed into a set of heliocentric distances \mathbf{r}_s ,

$$\mathbf{r}_s = N_r^{-1}(\mathbf{u}_r). \quad (21)$$

The size of the set is equal to the total number of objects, i.e. an integer value of $\max(N_r)$. Function N_r is obtained by numerical integration and it is in a discrete form, so the inversion has to be conducted by using some of the methods of inverse interpolation. All results presented in this paper were obtained by using the cubic spline interpolation. Further decreasing of the integration steps does not change results significantly. The obtained results also do not depend significantly on the choice of the interpolation method, especially when the integration steps in Eqs. 16, 20, 22, 23, 25 and 26 are small. The impact of the interpolation procedure is addressed in Section 5.1.

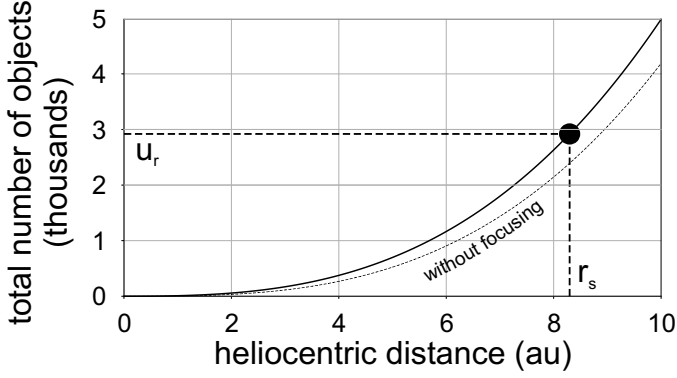


Figure 4: Total number of objects in the sphere around the Sun. The upper curve shows how the total number of ISOs increases if the radius of heliocentric sphere increases, assuming velocity distribution of interstellar velocities of M-stars (see Table 1) and interstellar number-density $n_0 = 1$. The curve representing corresponding number of objects without gravitational focusing is also given as a reference. This curve actually presents the variation of the volume of sphere with its radius. A schematic illustration of determining the heliocentric distance of a synthetic object (r_s) by using the inverse transform sampling method is also shown.

Step 2

Once the set of heliocentric distances \mathbf{r}_s is generated, the next step is to generate the corresponding set of interstellar velocities \mathbf{v}_{∞} . As pointed out earlier, this is done by inverting a probability function which is conditional with respect to already determined heliocentric distances, cumulative with respect to v_{∞} , and marginal with respect to other yet to be determined parameters. In order to sample from uniform random number $U(0, 1)$, the function has to be normalized to $p_r(r_s)$. For each element r_s from set \mathbf{r}_s this function is obtained by integration

$$p_{v_{\infty}cdf}(r_s) = \frac{1}{p_r(r_s)} \int_{v_{\infty(min)}}^{v_{\infty}} \int_0^{B_2} \int_0^{2\pi} \int_{-\frac{\pi}{2}}^{\frac{\pi}{2}} \int_0^{2\pi} p_6(r_s) dv_{\infty} dB dl db d\varphi \quad (22)$$

$$p_6(r_s) dv_{\infty} dB dl db d\varphi.$$

Interstellar velocities v_{∞} that correspond to every r_s from set \mathbf{r}_s are obtained by inverting this function,

$$v_{\infty} = p_{v_{\infty}cdf}(r_s)^{-1}(u_v), \quad u_v \sim U(0, 1).$$

As shown in Eq. 17, this function can be integrated analytically with respect to B and φ , while the integration with respect to v_{∞} , l and b is conducted numerically. Fig. 5 shows this function and schematic illustration of its inversion to obtain v_{∞} .

Step 3

After the sets of heliocentric distances \mathbf{r}_s and corresponding interstellar velocities \mathbf{v}_{∞} are determined, the impact parameters can be determined in an analogous manner. For each pair (r_s, v_{∞}) from these sets, corresponding B_s can be sampled from a probability function that is cumulative with respect to B , conditional with respect to r_s and v_{∞} , and marginal with respect to other parameters l , b and φ . Similar to the previous step, this function can be normalized to $p_{r,v_{\infty}}(r_s, v_{\infty})$, giving

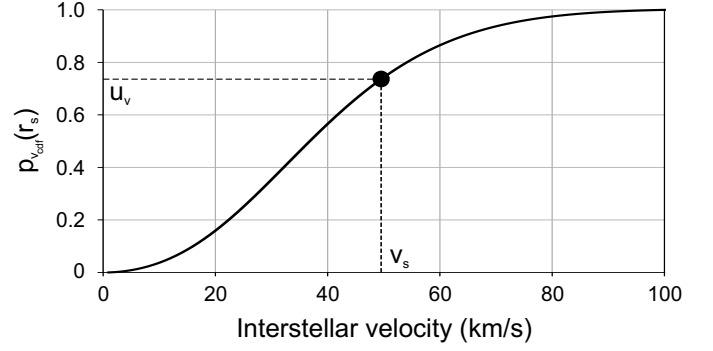


Figure 5: The cumulative distribution function of interstellar velocities for objects with defined heliocentric distance r_s , which is marginal with respect to impact parameters and longitudes and latitudes of the interstellar velocity vector. Schematic illustration of inverting this function to obtain v_{∞} is also shown.

$$p_{Bcdf}(r_s, v_{\infty}) = \frac{1}{p_{r,v_{\infty}}(r_s, v_{\infty})} \int_0^B \int_0^{2\pi} \int_{-\frac{\pi}{2}}^{\frac{\pi}{2}} \int_0^{2\pi} p_6(r_s, v_{\infty}) dB dl db d\varphi. \quad (23)$$

The corresponding impact parameter is obtained by inverting this function,

$$B_s = p_{Bcdf}(r_s, v_{\infty})^{-1}(u_B), \quad u_B \sim U(0, 1).$$

It should be noticed that function p_{Bcdf} has two forms depending on whether the object is the Sun-impactor or not (see Eq. 18). Which of these two forms is used is defined by the value of the random number u_B . If $u_B \leq p_{Bcdf}(r_s, v_{\infty}, B_1)$ then the object is the Sun-impactor and the first form of Eq. 17 is used. Otherwise, the object passes by the Sun and the second form is used (see also Eq. 4 and Fig. 1). In both cases, unlike inverting functions N_r and $p_{v_{\infty}cdf}$ to obtain r_s and v_{∞} , function $p_{Bcdf}(r_s, v_{\infty})$ can be inverted analytically giving the resulting impact parameter B_s in the form

$$B_s = \begin{cases} r_s \sqrt{f_1^2 - \left(\frac{f_1 p_v(v_{\infty}) - 2u_B}{p_v(v_{\infty})} \right)^2} & \text{if } u_B \leq p_{Bcdf}(r_s, v_{\infty}, B_1) \\ r_s \sqrt{f_1^2 - \left(\frac{f_2 p_v(v_{\infty}) - 2u_B}{2p_v(v_{\infty})} \right)^2} & \text{if } u_B > p_{Bcdf}(r_s, v_{\infty}, B_1) \end{cases}, \quad (24)$$

where

$$f_1 = \sqrt{1 + \frac{2\mu}{r_s v_{\infty s}^2}},$$

$$f_2 = \sqrt{1 + \frac{2\mu}{r_s v_{\infty s}^2}} + \sqrt{1 + \frac{2\mu}{r_s v_{\infty s}^2} - \left(\frac{R}{r_s}\right)^2 \left(1 + \frac{2\mu}{R v_{\infty s}^2}\right)}$$

Fig. 6 shows function $p_{B_{cdf}}$ and a schematic illustration of its inversion to obtain B_s .

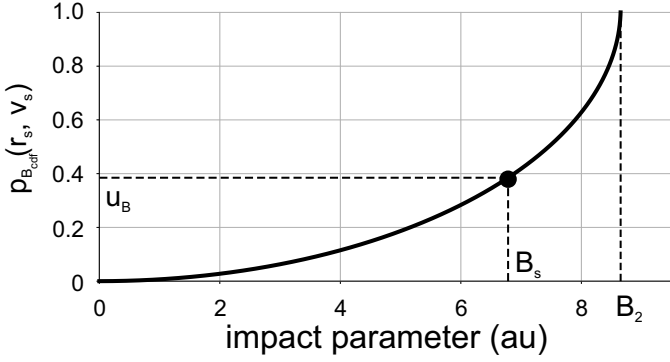


Figure 6: The cumulative distribution function of impact parameters, for objects with defined heliocentric distance r_s and interstellar velocity $v_{\infty s}$, which is marginal with respect to longitudes and latitudes of the interstellar velocity vector. Schematic illustration of inverting this function to obtain B_s is also shown.

Step 4

The next step is to determine the longitude of the interstellar velocity vector for each corresponding group of already determined parameters $(r_s, v_{\infty s}, B_s)$. This is obtained from a probability function that is cumulative with respect to l , conditional with respect to $r_s, v_{\infty s}$ and B_s , and marginal with respect to the remaining two still undetermined parameters b and φ . Again, this function can be normalized to $p_{r, v_{\infty}, B}(r_s, v_{\infty s}, B_s)$, giving

$$p_{l_{cdf}}(r_s, v_{\infty s}, B_s) = \frac{1}{p_{r, v_{\infty}, B}(r_s, v_{\infty s}, B_s)} \int_0^l \int_{-\frac{\pi}{2}}^{\frac{\pi}{2}} \int_0^{2\pi} p_6(r_s, v_{\infty s}, B_s) dl db d\varphi \quad (25)$$

$$p_6(r_s, v_{\infty s}, B_s) dl db d\varphi.$$

As in all previous step, this function can be integrated analytically with respect to φ , while the integration with respect to l and b has to be conducted numerically. Longitude of the interstellar velocity vector is obtained by inverting this function

$$l_s = p_{l_{cdf}}(r_s, v_{\infty s}, B_s)^{-1}(u_l), \quad u_l \sim U(0, 1).$$

Fig. 7 shows this function and schematic illustration of its inversion to obtain l_s .

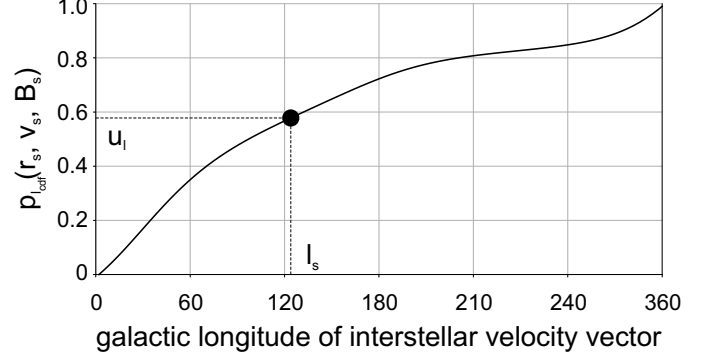


Figure 7: The cumulative distribution function of longitude of interstellar velocity vector, for objects with defined heliocentric distance r_s , interstellar velocity $v_{\infty s}$ and impact parameter B_s , which is marginal with respect to latitudes of the interstellar velocity vector. Schematic illustration of inverting this function to obtain l_s is also shown.

Step 5

The fifth step is to determine latitude of the interstellar velocity vector for every corresponding group of already determined parameters $(r_s, v_{\infty s}, B_s, l_s)$. This is obtained from a probability function which is cumulative with respect to b , conditional with respect to $r_s, v_{\infty s}, B_s$ and l_s and marginal with respect to the remaining undetermined parameter φ . As in all previous steps, this function can be normalized to $p_{r, v_{\infty}, B, l}(r_s, v_{\infty s}, B_s, l_s)$, giving

$$p_{b_{cdf}}(r_s, v_{\infty s}, B_s, l_s) = \frac{1}{p_{r, v_{\infty}, B, l}(r_s, v_{\infty s}, B_s, l_s)} \int_{-\frac{\pi}{2}}^b \int_0^{2\pi} p_6(r_s, v_{\infty s}, B_s, l_s) db d\varphi. \quad (26)$$

This function can be integrated analytically with respect to φ (see Eq. 23), while the integration with respect to b has to be conducted numerically. Latitude of the interstellar velocity vector is obtained by inverting this function

$$b_s = p_{b_{cdf}}(r_s, v_{\infty s}, B_s, l_s)^{-1}(u_b), \quad u_b \sim U(0, 1).$$

Fig. 8 shows this function and schematic illustration of its inversion to obtain b_s .

Step 6

The last step is to determine angle φ . As mentioned earlier, the joint probability function p_6 does not depend on this angle, which means that it can simply be sampled from a uniform distribution $\varphi \sim U(0, 2\pi)$.

5. Results and discussion

The *Probabilistic method* is applied to generate synthetic populations of ISOs assuming different distributions of interstellar. The resulting populations are compared to those generated by

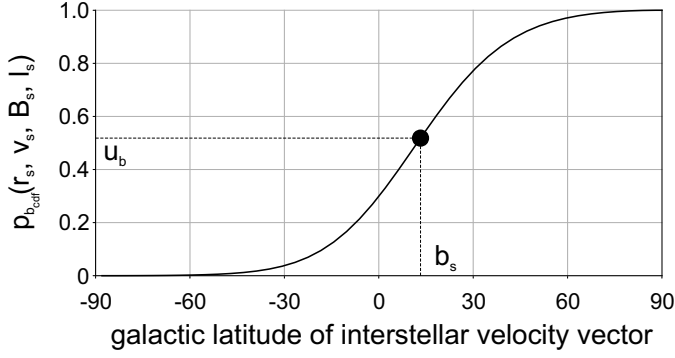


Figure 8: The cumulative distribution function of latitude of interstellar velocity vector, for objects with defined heliocentric distance r_s , interstellar velocity $v_{\infty S}$, impact parameter B_s and longitude l_s . Schematic illustration of inverting this function to obtain b_s is also shown.

the *Dynamical methods* and numerical integration in order to analyse its ability to generate realistic populations and its computational performances.

5.1. Sensitivity of the ISO population on the assumed distribution of interstellar velocities

To demonstrate the sensitivity of the ISO population to the assumed distribution of interstellar velocities, the *Probabilistic method* was used to generate synthetic populations of ISOs within a heliocentric sphere of radius 50 au, for three different distributions of interstellar velocities defined in Table 1. Histograms of 6 orbital elements of the obtained synthetic populations are shown in Fig. 9.

Fig. 9 shows that the O/B-stars kinematics, due to the smaller velocity component dispersions, results in the largest number of objects, which in this case is 577177, compared to 555009 and 542266 for the G- and M-stars kinematics, respectively. This can be seen most clearly in histograms of perihelion distances, orbital inclinations and true anomalies. In addition, there are noticeable differences in the distributions of eccentricity, argument of perihelion, and longitude of ascending node. The orbits of the population with the kinematics of O/B stars are distributed over a much smaller range of eccentricities. The mean eccentricity values are around 20, 49 and 64 for the populations with O/B, G and M-star kinematics, respectively. In addition, there are noticeable differences in the distributions of the argument of perihelion ω and longitude of ascending node Ω , especially for the population with O/B kinematics which has more pronounced variations. The velocity dispersions of the kinematics of O/B-stars are the smallest and consequently, the corresponding distributions of ω and Ω are most affected by the solar motion with respect to the LSR. Consequently, the objects that originate from these stars are probably more likely to be captured by the solar system.

As mentioned earlier, the results reported in Fig. 9 were obtained using cubic spline interpolation. The *Probabilistic method* can be easily adjusted to use any other interpolation method. However, it should not lead to significant change of the results. For example, Fig. 10 shows comparison of distributions of argument of perihelion using cubic spline and simple

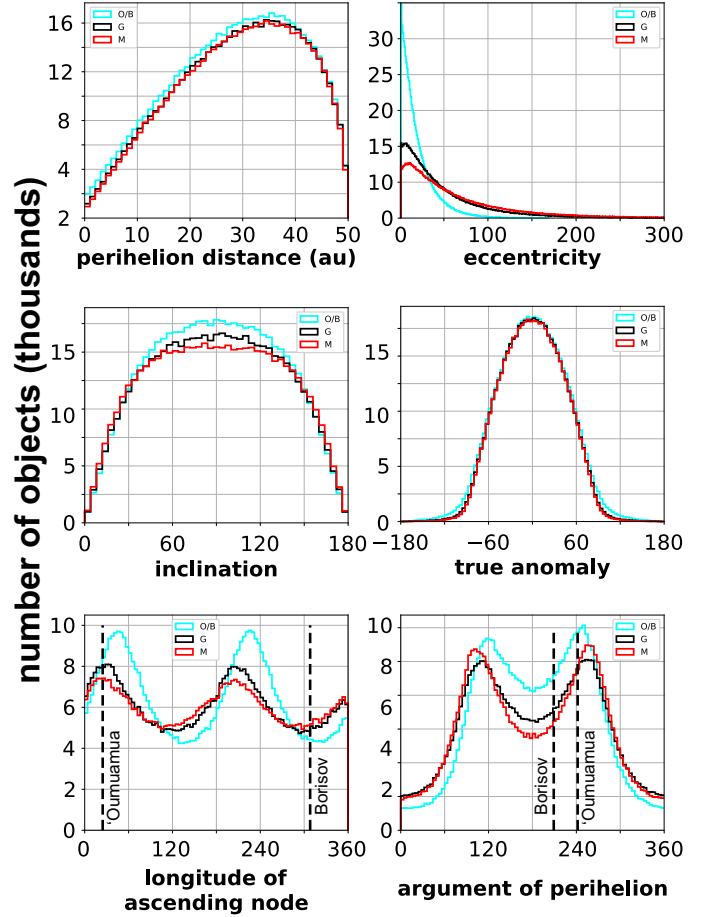


Figure 9: Distributions of orbital elements of ISOs within a heliocentric sphere of radius 50 au, assuming kinematics of stellar classes M, G and O/B (see Table 1). For reference, vertical lined denoting 1I/Oumuamua and 2I/Borisov are given on the plots for argument of perihelion and longitude of ascending node, the two orbital elements likely least affected by observational selection effects.

linear interpolation. Although the steps in this case were much larger ($\Delta v = 2$ km/s, $\Delta r = 1$ au, $\Delta l = \Delta b = 4^\circ$), the obtained results are very consistent since cosine similarity between the two histograms shown in Fig. 10 is ~ 0.999 .

Fig. 11 shows distribution of the incoming directions of ISOs, assuming the kinematics of M-stars (see Table 1). The majority of objects come from the region near the solar apex. The densest region is slightly shifted toward the galactic center due to the greater dispersion of U-components of the interstellar velocity vectors.

The comparison of these three cases shows how important it is to have an adequate assumption about the interstellar velocity distribution of ISOs in order to synthesize their realistic population. The interstellar kinematics of ISOs may depend not only on the global kinematics of the stars in the solar neighborhood, but also on the relative contribution of different stellar classes to this population. In this way, the ISO kinematics may result from a specific mixture of stellar kinematics. When a sufficient number of ISOs are discovered to reconstruct their orbital structure in the Solar System, it could give an indication of the contribution of different stellar classes to the galactic population of these

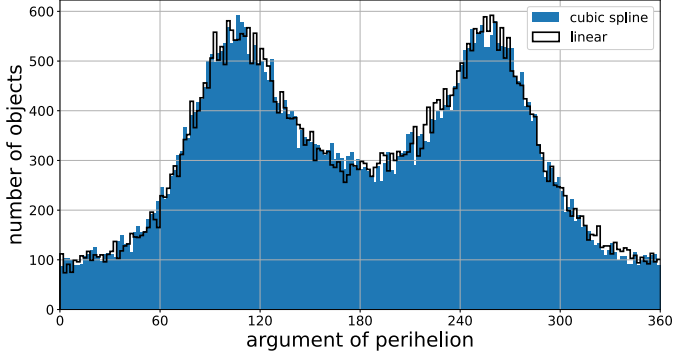


Figure 10: Comparison of distributions of argument of perihelion obtained using cubic spline and linear interpolation.

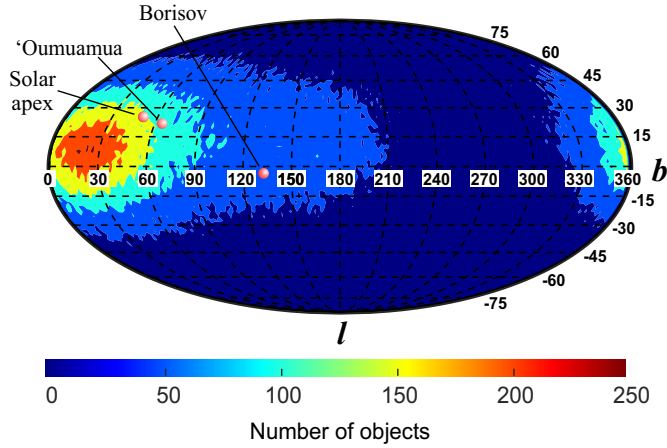


Figure 11: Distribution of incoming directions of ISOs in the galactic reference frame for the synthetic population inside model sphere with radius of 50 au, number-density of 1 object per au^3 and kinematics of M-stars (table 1)

objects. As it is shown in Section 5.2, the *Probabilistic method* is very computationally efficient, so it can be used to generate a large number of synthetic populations with a variety of input kinematics. In this way, one can infer which mixture resulted in the actual population, thus indicating the relative contributions of the different stellar classes to the ISO population.

5.2. Comparison of Probabilistic and Dynamical methods

In order to cross-check the results obtained by the *Dynamical* and *Probabilistic* methods, a comparison was made for the populations generated within the model sphere with a radius of 50 au, number-density of 1 object per au^3 and the kinematics of M-stars (see table 1). The obtained distributions of orbital elements are practically indistinguishable. To quantify the consistency of the results, the cosine similarities of the corresponding histograms were calculated and none were below 0.999, regardless of the bin size. For visual comparison, histograms of argument of perihelion is shown in Fig. 12.

As mentioned earlier, there are two main advantages of the *Probabilistic* over the *Dynamical methods*. One refers to accuracy of the synthesized population, i.e. how well it corresponds to the input distribution of interstellar velocities, while the other one refers to computational efficiency.

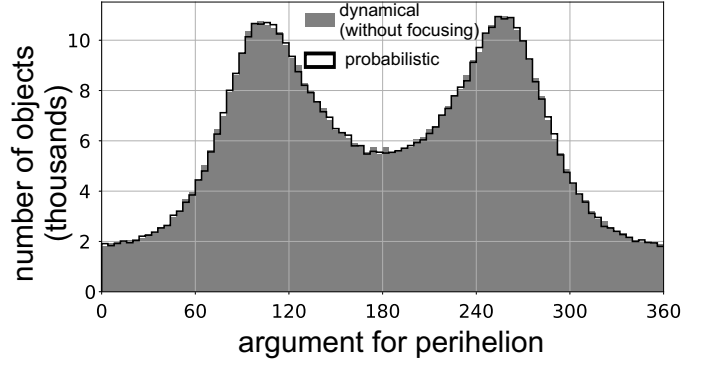


Figure 12: Histograms of argument of perihelion obtained by the *Probabilistic method* and *Dynamical method (without focusing)*.

The *Dynamical method (without focusing)* is accurate enough only if it is used to generate a synthetic population in a sufficiently large heliocentric sphere. If the population is generated in a small heliocentric sphere, it underestimates the total number of objects, and the population is also biased toward faster objects. This means that even a realistic kinematics of ISOs in interstellar space is provided, the resulting synthetic population will deviate systematically from the real population. As previously discussed, this is due to the fact that the *Dynamical method (without focusing)* assumes that outside the sphere where the population is generated, the gravitational focusing is neglected and the number-density is equal to that in interstellar space. However, as illustrated in Fig. 3, this effect affects the population at large heliocentric distances and its neglect leads to certain underestimation of the number of objects in the inner Solar System. On the other hand, *Dynamical method (with focusing)* takes this effect into account, but leaves the directions of the initial velocity vectors unaffected by the solar gravity. To quantify the influence of these effects, synthetic populations were generated using the *Dynamical* and *Probabilistic methods* within the model spheres of radii from 0.5 au to 15 au, with a step of 0.25 au. The populations were generated assuming velocity distribution of M-stars (see Table 1) and the results are reported in Fig. 13.

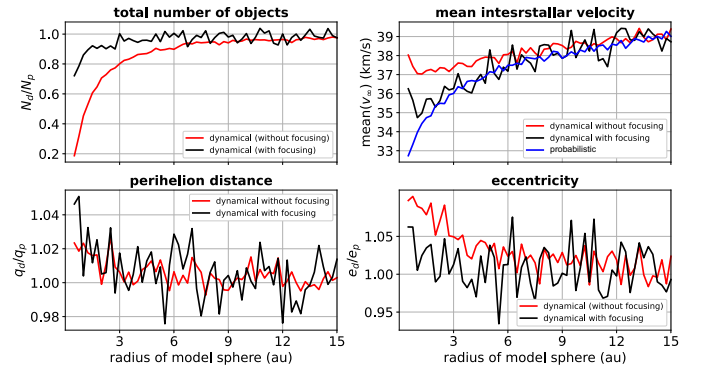


Figure 13: Comparison of parameters of populations generated using the *Probabilistic* and *Dynamical methods*.

Fig. 13 (top-left panel) shows, that the *Dynamical method*

(without focusing) significantly underestimates the total number of objects for populations generated in small model spheres, but this number closely approaches that of the *Probabilistic method* for populations created within a heliocentric sphere with a radius greater than about 10 au. On the other hand, *Dynamical method (without focusing)* shows much better agreement with the *Probabilistic method*, resulting in practically the same number of objects for model spheres with radii larger than 3 au.

As previously discussed, gravitational focusing affects stronger objects with lower interstellar velocities and ignoring it leads not only to underestimating the total number of objects, but also to changing the population structure by reducing the relative participation of slower objects. Fig. 13 (top-right panel) shows mean interstellar velocities for populations generated using the *Probabilistic* and *Dynamical* methods in model spheres with radii ranging from 0.5 to 15 au. In this case, *Dynamical method (with focusing)* shows excellent agreement with the *Probabilistic method*, while the *Dynamical method (without focusing)* has larger values at small heliocentric distances due to the bias toward faster objects. Underestimation of slower objects is significant because they are very important (e.g. they have the highest probability to be captured by some of the dynamical mechanisms (Dehnen and Hands, 2021; Napier et al., 2021a,b)).

The bottom two panels in Fig. 13 show deviation of mean perihelion distance and mean eccentricity for populations generated by the *Dynamical methods* from the one generated using the *Probabilistic method*. Again, as expected, *Dynamical method (with focusing)* has much better agreement. However, as mentioned earlier, although this method accounts for the gravitational focusing outside the model sphere, and adjusts the initial speeds for the solar acceleration, it ignores the fact that the directions of the velocity vectors at an arbitrary heliocentric distance are not identical to the corresponding directions at infinity. This gives the orbits a slightly larger angular momentum, and therefore a slightly higher eccentricity and perihelion distance.

Fig. 13 shows that populations generated using the *Dynamical method* converge to those generated using the *Probabilistic method* if the heliocentric distance increases. As a consequence, if a population of ISOs is generated using the *Dynamical methods*, it has to be generated within a large model sphere, beyond which the effect of gravitational focusing can be safely ignored. For example, if one needs a synthetic population of ISOs around the Earth’s orbit, the population has to be generated in a much larger volume of space and then the relevant objects from that population have to be selected.

Another advantage of the *Probabilistic method* relates to its computational efficiency, since it is significantly faster than the *Dynamical method*. Fig. 14 shows the ratio of the times required to generate synthetic populations by *Dynamical method* (t_d) and *Probabilistic method* (t_s), depending on the radius of the model sphere.

As Fig. 14 illustrates, this ratio increases with the increased volume of space where the synthetic population is generated, reaching three orders of magnitude for a model sphere with radius of 100 au. Analysing ISO populations usually requires syn-

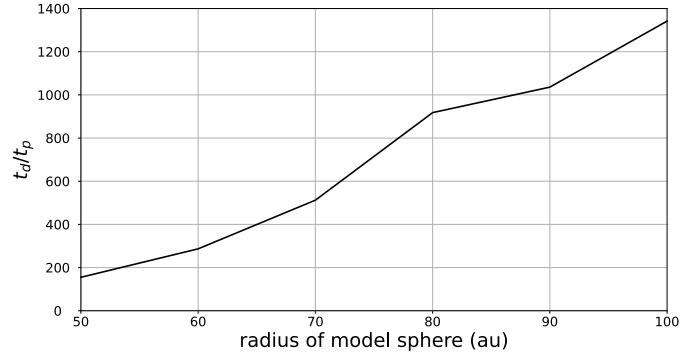


Figure 14: Comparison of the times required to generate synthetic populations using *Dynamical method (with focusing)* (t_d) and *Probabilistic method* (t_s). Due to the very large computational demand of the *Dynamical method*, these data were obtained by generating populations assuming very small number-density $n_0 = 10^{-3}$ object per au^3 .

thetic populations within such large heliocentric spheres. For example, Engelhardt et al. (2017) and Marčeta and Novaković (2020) analysed synthetic populations inside model spheres with radii 50 au and 100 au, respectively. The reason for this was that objects within these spheres are capable of reaching heliocentric distances at which they could be detected by the LSST survey during the defined nominal duration of this survey of 10 years (LSST Science Collaboration et al., 2017). With this in mind, the computational efficiency of the procedure becomes very important for the possibility of its systematic implementation. The computational efficiency of the *Probabilistic method* depends on the choice of the integration steps in Eqs. 16, 20, 22, 23, 25 and 26. Steps $dr = 10^{-3}$ au, $dv = 1$ km/s, $dl = db = 1^\circ$ were used for the comparison reported in Fig. 14. Further decreasing of the integration steps does not lead to a significant change of the results, as previously discussed in Section 4. On the other hand, most of the computational load in the *Dynamical methods* goes to the generation of initial Cartesian state vectors and their conversion to orbital elements and solving the hyperbolic Kepler equation for a large number of the initial objects. Adjusting the tolerance for numerical solving of this equation can change the computational efficiency of the method to a lesser extent, since the numerical schemes for solving the hyperbolic Kepler equation converge very quickly.

5.3. Limitations of the Probabilistic method

The *Probabilistic method* is completely heliocentric, which means that it takes into account only the gravitational influence of the Sun on ISOs and ignores the influence of the planets. However, when an ISO enters the Solar System it is initially governed by barycentric attraction. Analyses of long-period comet orbits show that this can be good approximation up to heliocentric distances of about 150-200 au (Todorovic-Juchniewicz, 1981; Fouchard et al., 2017). In order to accurately track the orbit of the object at smaller heliocentric distances, perturbational effect of the planets has to be taken into account, as well as non-gravitational effects for comets at some point. In addition, close approach to the giant planets, especially Jupiter, can significantly change the orbital elements of the object (e.g. Branham,

2013; Buffoni et al., 1982). However, although these effects can have significant impact on a particular orbit, their impact on the orbital structure of ISOs in the Solar System is negligible. To demonstrate this, a population of ISOs is generated with the *Probabilistic method* and compared to the population generated by numerical integration using Rebound ias15 numerical integrator (Rein and Spiegel, 2015), with all 8 planets included in the dynamical model. To obtain the population using numerical integration, the initial positions and velocity vectors were obtained in the same way as in the *Dynamical method (without focusing)*. After that, the orbits were propagated by numerical integration that takes into account the full dynamical model, instead of solving the hyperbolic Kepler equation for each object, as in the *Dynamical Model*. The populations were generated assuming M-stars kinematics (table 1).

Fig. 15 shows the resulting histograms of perihelion distance obtained by the *Probabilistic method* and numerical integration.

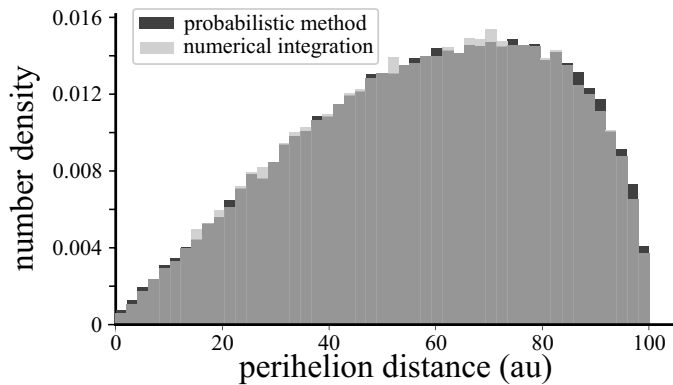


Figure 15: Normalised histograms of perihelion distance obtained by the *Probabilistic method* and numerical integration.

As Fig. 15 illustrates, the distributions of perihelion distance obtained by the *Probabilistic method* and numerical integration are practically indistinguishable. The cosine similarity for these two histograms is ~ 0.999 . This shows that planetary perturbations, although capable of changing a particular orbit significantly, cannot change the probability distributions of the orbital elements, so their impact on the orbital structure of instantaneous population of ISOs is negligible.

6. Summary and Conclusions

The 6-variate distribution of parameters defining orbits ISOs in the Solar System is derived. This distribution is used as a basis for the development of the so-called *Probabilistic method* for generating the synthetic populations of ISOs.

The main conclusions can be summarised as follows:

1. The effect of gravitational focusing defines the orbital structure of the population of interstellar objects around the Sun. The intensity of this effect depends on the assumed distribution of interstellar velocities of these objects. For the reasonable assumptions of these distributions, it increases number-density of ISOs by about factor of 2 around the Earth's orbit, and by order of magnitude at very small heliocentric distances.
2. At very small heliocentric distances comparable to the Solar radius, the physical size of the Sun causes the so-called shielding effect, which results in a decrease of ISOs number-density. This space is populated only with interstellar Sun-impactors.
3. The developed *Probabilistic method* for generating synthetic populations of ISOs fully takes into account the effect of gravitational focusing, regardless of the radius of the sphere where the synthetic population is generated. This characteristic makes it suitable for generating synthetic population in small model spheres. In contrast, the *Dynamical methods* underestimates the total number of objects when used to generate a synthetic population in small heliocentric spheres.
4. The *Dynamical methods* underestimates the number of slower objects in the populations. This shortcoming is significantly overcome by taking into account the gravitational focusing outside the sphere in which the synthetic population is generated. To entirely overcome this issue, the population using the *Dynamical methods* has to be generated in a sufficiently large model sphere beyond which the effect of gravitational focusing can be safely ignored. On the other hand, the *Probabilistic method* is independent of the size of the model sphere.
5. The *Probabilistic method* is significantly more efficient than the *Dynamical methods*. The difference in efficiency depends on the size of the model sphere where the synthetic population is generated and reaches three orders of magnitude for a model sphere with radius of 100 au, depending on the numerical parameters involved in these two methods. High efficiency of the *Probabilistic method* allows its systematic use for exploration of possible populations of ISOs.

Data Availability Statement

The Python code that implements the developed *Probabilistic method* for generating the synthetic population of ISOs is available within *Astronomy Source Code Library ASCL* at <https://ascl.net/2209.014>. The code includes Python libraries *NumPy* (Harris et al., 2020), *SciPy* (Virtanen et al., 2020), *Random* (Van Rossum, 2020) and *tqdm* (da Costa-Luis, 2019).

References

- Beard, D.B., 1959. Interplanetary Dust Distribution. *The Astrophysical Journal* 129, 496.
- Binney, J., Michael, M., 1998. *Galactic Astronomy*. Princeton Univ. Press.
- Bland-Hawthorn, J., Gerhard, O., 2016. The Galaxy in Context: Structural, Kinematic, and Integrated Properties. *Annual Review of Astronomy and Astrophysics* 54, 529–596. doi:10.1146/annurev-astro-081915-023441, arXiv:1602.07702.
- Borisov, G., 2019. 2019-R106. *Minor Planet Electronic Circulars*.
- Bortle, J.E., 1991. Post-Perihelion Survival of Comets with Small q . *International Comet Quarterly* 13, 89.

- Branham, R. L., J., 2013. New Orbits for Comets C/1960 M1 (Humason), C/1980 E1 (Bowell), and Musings on Extrasolar Comets. *Revista Mexicana de Astronomía y Astrofísica* 49, 111–116.
- Buffoni, L., Scardia, M., Manara, A., 1982. The orbital evolution of comet Bowell (1980b). *Moon and Planets* 26, 311–315. doi:10.1007/BF00928013.
- Childs, A.C., Martin, R.G., 2022. Misaligned Circumbinary Disks as Efficient Progenitors of Interstellar Asteroids. *The Astrophysical Journal Letters* 935, L31. doi:10.3847/2041-8213/ac8880, arXiv:2208.05874.
- Colombo, G., Lautman, D.A., Shapiro, I.I., 1966. The earth's dust belt: Fact or fiction?: 2. gravitational focusing and jacobini capture. *Journal of Geophysical Research* 71, 5705–5717.
- da Costa-Luis, C.O., 2019. 'tqdm': A fast, extensible progress meter for python and cli. *Journal of Open Source Software* 4, 1277. URL: <https://doi.org/10.21105/joss.01277>, doi:10.21105/joss.01277.
- Čuk, M., 2018. 1I/ʻOumuamua as a Tidal Disruption Fragment from a Binary Star System. *The Astrophysical Journal Letters* 852, L15. doi:10.3847/2041-8213/aaa3db, arXiv:1712.01823.
- Dehnen, W., Hands, T.O., 2021. Capture of interstellar objects I: the capture cross-section. *Monthly Notices of the Royal Astronomical Society* doi:10.1093/mnras/stab3670, arXiv:2112.07468.
- Dehnen, W., Hands, T.O., Schönrich, R., 2021. Capture of interstellar objects II: by the Solar system. *Monthly Notices of the Royal Astronomical Society* doi:10.1093/mnras/stab3666, arXiv:2112.07486.
- Devroye, L., 1986. *Non-Uniform Random Variate Generation*. Springer-Verlag.
- Do, A., Tucker, M.A., Tonry, J., 2018. Interstellar Interlopers: Number Density and Origin of ʻOumuamua-like Objects. *The Astrophysical Journal Letters* 855, L10. doi:10.3847/2041-8213/aaae67, arXiv:1801.02821.
- Engelhardt, T., Jedicke, R., Vereš, P., Fitzsimmons, A., Denneau, L., Beshore, E., Meinke, B., 2017. An Observational Upper Limit on the Interstellar Number Density of Asteroids and Comets. *The Astronomical Journal* 153, 133. doi:10.3847/1538-3881/aa5c8a, arXiv:1702.02237.
- Fitzsimmons, A., Snodgrass, C., Rozitis, B., Yang, B., Hyland, M., Secull, T., Bannister, M.T., Fraser, W.C., Jedicke, R., Lacerda, P., 2018. Spectroscopy and thermal modelling of the first interstellar object 1I/ʻOumuamua. *Nature Astronomy* 2, 133–137. doi:10.1038/s41550-017-0361-4, arXiv:1712.06552.
- Fouchard, M., Rickman, H., Froeschlé, C., Valsecchi, G.B., 2017. Distribution of long-period comets: comparison between simulations and observations. *Astronomy & Astrophysics* 604, A24. doi:10.1051/0004-6361/201630343.
- Granvik, M., Morbidelli, A., Jedicke, R., Bolin, B., Bottke, W.F., Beshore, E., Vokrouhlický, D., Nesvorný, D., Michel, P., 2018. Debaised orbit and absolute-magnitude distributions for near-Earth objects. *Icarus* 312, 181–207. doi:10.1016/j.icarus.2018.04.018, arXiv:1804.10265.
- Grav, T., Jedicke, R., Denneau, L., Chesley, S., Holman, M.J., Spahr, T.B., 2011. The Pan-STARRS Synthetic Solar System Model: A Tool for Testing and Efficiency Determination of the Moving Object Processing System. *Publications of the Astronomical Society of the Pacific* 123, 423. doi:10.1086/659833.
- Greenstreet, S., Ngo, H., Gladman, B., 2012. The orbital distribution of Near-Earth Objects inside Earth's orbit. *Icarus* 217, 355–366. doi:10.1016/j.icarus.2011.11.010.
- Gronchi, G.F., Baù, G., Rodríguez, Ó., Jedicke, R., Moeyens, J., 2021. Generalization of a method by Mossotti for initial orbit determination. *Celestial Mechanics and Dynamical Astronomy* 133, 41. doi:10.1007/s10569-021-10038-4, arXiv:2104.00345.
- Hale, D.P., Wright, J.J., 1964. Meteoric Flux and Density Fields about a Finite Attractive Center Generated by a Stream Monoenergetic and Monodirectional at Infinity. *Journal of Geophysical Research* 69, 3719–3726.
- Harris, C.R., Millman, K.J., van der Walt, S.J., Gommers, R., Virtanen, P., Cournapeau, D., Wieser, E., Taylor, J., Berg, S., Smith, N.J., Kern, R., Picus, M., Hoyer, S., van Kerkwijk, M.H., Brett, M., Haldane, A., del Río, J.F., Wiebe, M., Peterson, P., Gérard-Marchant, P., Sheppard, K., Reddy, T., Weckesser, W., Abbasi, H., Gohlke, C., Oliphant, T.E., 2020. Array programming with NumPy. *Nature* 585, 357–362. URL: <https://doi.org/10.1038/s41586-020-2649-2>, doi:10.1038/s41586-020-2649-2.
- Hoover, D.J., Seligman, D.Z., Payne, M.J., 2022. The Population of Interstellar Objects Detectable with the LSST and Accessible for In Situ Rendezvous with Various Mission Designs. *The Planetary Science Journal* 3, 71. doi:10.3847/PSJ/ac58fe, arXiv:2109.10406.
- Jackson, A.P., Tamayo, D., Hammond, N., Ali-Dib, M., Rein, H., 2018. Ejection of rocky and icy material from binary star systems: implications for the origin and composition of 1I/ʻOumuamua. *Monthly Notices of the Royal Astronomical Society* 478, L49–L53. doi:10.1093/mnras/1/sly033, arXiv:1712.04435.
- Jewitt, D., Luu, J., Rajagopal, J., Kotulla, R., Ridgway, S., Liu, W., Augusteijn, T., 2017. Interstellar Interloper 1I/2017 U1: Observations from the NOT and WIYN Telescopes. *The Astrophysical Journal Letters* 850, L36. doi:10.3847/2041-8213/aa9b2f, arXiv:1711.05687.
- Jewitt, D., Seligman, D.Z., 2022. The Interstellar Interlopers. arXiv e-prints, arXiv:2209.08182arXiv:2209.08182.
- Kemble, S., 2006. *Interplanetary Mission Analysis and Design*. Praxis Publishing Ltd.
- Knight, M.M., Walsh, K.J., 2013. Will Comet ISON (C/2012 S1) Survive Perihelion? *The Astrophysical Journal Letters* 776, L5. doi:10.1088/2041-8205/776/1/L5, arXiv:1309.2288.
- Laughlin, G., Batygin, K., 2017. On the Consequences of the Detection of an Interstellar Asteroid. *Research Notes of the American Astronomical Society* 1, 43. doi:10.3847/2515-5172/aaa02b, arXiv:1711.02260.
- Levine, W.G., Cabot, S.H.C., Seligman, D., Laughlin, G., 2021. Constraints on the Occurrence of ʻOumuamua-Like Objects. *The Astrophysical Journal* 922, 39. doi:10.3847/1538-4357/ac1fe6, arXiv:2108.11194.
- LSST Science Collaboration, Marshall, P., Anguita, T., Bianco, F.B., Bellm, E.C., Brandt, N., Clarkson, W., Connolly, A., Gawiser, E., Ivezić, Z., Jones, L., Lochner, M., Lund, M.B., Mahabal, A., Nidever, D., Olsen, K., Ridgway, S., Rhodes, J., Shemmer, O., Trilling, D., Vivas, K., Walkowicz, L., Willman, B., Yoachim, P., Anderson, S., Antilogus, P., Angus, R., Arcavi, I., Awan, H., Biswas, R., Bell, K.J., Bennett, D., Britt, C., Buzasi, D., Casetti-Dinescu, D.I., Chomiuk, L., Claver, C., Cook, K., Davenport, J., Debattista, V., Digel, S., Doctor, Z., Firth, R.E., Foley, R., Fong, W.f., Galbany, L., Giampapa, M., Gizis, J.E., Graham, M.L., Grillmair, C., Gris, P., Haiman, Z., Hartigan, P., Hawley, S., Hlozek, R., Jha, S.W., Johns-Krull, C., Kanbur, S., Kalogera, V., Kashyap, V., Kasliwal, V., Kessler, R., Kim, A., Kurczynski, P., Lahav, O., Liu, M.C., Malz, A., Margutti, R., Matheson, T., McEwen, J.D., McGehee, P., Meibom, S., Meyers, J., Monet, D., Neilsen, E., Newman, J., O'Dowd, M., Peiris, H.V., Penny, M.T., Peters, C., Poleski, R., Ponder, K., Richards, G., Rho, J., Rubin, D., Schmidt, S., Schuhmann, R.L., Shporer, A., Slater, C., Smith, N., Soares-Santos, M., Stassun, K., Strader, J., Strauss, M., Street, R., Stubbs, C., Sullivan, M., Szkody, P., Trimble, V., Tyson, T., de Val-Borro, M., Valenti, S., Wagoner, R., Wood-Vasey, W.M., Zauderer, B.A., 2017. Science-Driven Optimization of the LSST Observing Strategy. arXiv e-prints, arXiv:1708.04058arXiv:1708.04058.
- Marčeta, D., Novaković, B., 2020. Retrograde orbits excess among observable interstellar objects. *Monthly Notices of the Royal Astronomical Society* 498, 5386–5398. doi:10.1093/mnras/staa1378, arXiv:2005.10236.
- Moore, K., Courville, S., Ferguson, S., Schoenfeld, A., Llera, K., Agrawal, R., Brack, D., Buhler, P., Connour, K., Czaplinski, E., DeLuca, M., Deutsch, A., Hammond, N., Kuettel, D., Marusiak, A., Nerozzi, S., Stuart, J., Tarnas, J., Thelen, A., Castillo-Rogez, J., Smythe, W., Landau, D., Mitchell, K., Budney, C., 2021. Bridge to the stars: A mission concept to an interstellar object. *Planetary and Space Science* 197, 105137. doi:10.1016/j.pss.2020.105137.
- Morbidelli, A., Batygin, K., Brasser, R., Raymond, S.N., 2020. No evidence for interstellar planetesimals trapped in the Solar system. *Monthly Notices of the Royal Astronomical Society* 497, L46–L49. doi:10.1093/mnras/1/slaa111, arXiv:2006.04534.
- Moro-Martín, A., Norman, C., 2022. Interstellar Planetesimals: Potential Seeds for Planet Formation? *The Astrophysical Journal* 924, 96. doi:10.3847/1538-4357/ac32cc, arXiv:2110.15366.
- Moro-Martín, A., Turner, E.L., Loeb, A., 2009. Will the Large Synoptic Survey Telescope Detect Extra-Solar Planetesimals Entering the Solar System? *The Astrophysical Journal* 704, 733–742. doi:10.1088/0004-637X/704/1/733, arXiv:0908.3948.
- Namouni, F., Morais, M.H.M., 2020. An interstellar origin for high-inclination Centaurs. *Monthly Notices of the Royal Astronomical Society* 494, 2191–2199. doi:10.1093/mnras/staa712, arXiv:2004.10510.
- Napier, K.J., Adams, F.C., Batygin, K., 2021a. On the Capture of Interstellar Objects by Our Solar System. *The Planetary Science Journal* 2, 53. doi:10.3847/PSJ/abe76e/53, arXiv:2102.08488.
- Napier, K.J., Adams, F.C., Batygin, K., 2021b. On the Fate of Interstellar Objects Captured by Our Solar System. *The Planetary Science Journal* 2, 217. doi:10.3847/PSJ/ac29bb, arXiv:2109.11017.

- Pfalzner, S., Aizpuru Vargas, L.L., Bhandare, A., Veras, D., 2021. Significant interstellar object production by close stellar flybys. *Astronomy & Astrophysics* 651, A38. doi:10.1051/0004-6361/202140587, arXiv:2104.06845.
- Pfalzner, S., Bannister, M.T., 2019. A Hypothesis for the Rapid Formation of Planets. *The Astrophysical Journal Letters* 874, L34. doi:10.3847/2041-8213/ab0fa0, arXiv:1903.04451.
- Phan, V.H.M., Hoang, T., Loeb, A., 2021. Erosion of Icy Interstellar Objects by Cosmic Rays and Implications for 'Oumuamua. arXiv e-prints, arXiv:2109.04494 arXiv:2109.04494.
- Rein, H., Spiegel, D.S., 2015. IAS15: a fast, adaptive, high-order integrator for gravitational dynamics, accurate to machine precision over a billion orbits. *Monthly Notices of the Royal Astronomical Society* 446, 1424–1437. doi:10.1093/mnras/stu2164, arXiv:1409.4779.
- Schwamb, M.E., Jurić, M., Bolin, B.T., Dones, L., Greenstreet, S., Hsieh, H.H., Inno, L., Jones, R.L., Kelley, M.S.P., Knight, M.M., Reach, W.T., Seccull, T., Snodgrass, C., Trilling, D.E., Vera C. Rubin Observatory LSST Solar System Science Collaboration, 2021. Year 1 of the Legacy Survey of Space and Time (LSST): Recommendations for Template Production to Enable Solar System Small Body Transient and Time Domain Science. *Research Notes of the American Astronomical Society* 5, 143. doi:10.3847/2515-5172/ac090f.
- Seligman, D., Laughlin, G., 2018. The Feasibility and Benefits of In Situ Exploration of 'Oumuamua-like Objects. *The Astronomical Journal* 155, 217. doi:10.3847/1538-3881/aabd37, arXiv:1803.07022.
- Seligman, D.Z., Rogers, L.A., Cabot, S.H.C., Noonan, J.W., Kareta, T., Mandt, K.E., Ciesla, F., McKay, A., Feinstein, A.D., Levine, W.G., Bean, J.L., Nordlander, T., Krumholz, M.R., Mansfield, M., Hoover, D.J., Van Clepper, E., 2022. The Volatile Carbon-to-oxygen Ratio as a Tracer for the Formation Locations of Interstellar Comets. *The Planetary Science Journal* 3, 150. doi:10.3847/PSJ/ac75b5, arXiv:2204.13211.
- Silsbee, K., Tremaine, S., 2016. Modeling the Nearly Isotropic Comet Population in Anticipation of LSST Observations. *The Astronomical Journal* 152, 103. doi:10.3847/0004-6256/152/4/103, arXiv:1607.07882.
- Singer, S.F., 1961. Interplanetary Dust near the Earth. *Nature* 192, 321–323.
- Snodgrass, C., Jones, G.H., 2019. The European Space Agency's Comet Interceptor lies in wait. *Nature Communications* 10, 5418. doi:10.1038/s41467-019-13470-1.
- Tedesco, E.F., Cellino, A., Zappalá, V., 2005. The Statistical Asteroid Model. I. The Main-Belt Population for Diameters Greater than 1 Kilometer. *The Astronomical Journal* 129, 2869–2886. doi:10.1086/429734.
- Todorovic-Juchniewicz, B., 1981. When we may and Need to Use Barycentric Orbit of a Comet. *Acta Astronomica* 31, 191.
- Trilling, D.E., Robinson, T., Roegge, A., Chandler, C.O., Smith, N., Loeffler, M., Trujillo, C., Navarro-Meza, S., Glaspie, L.M., 2017a. Implications for Planetary System Formation from Interstellar Object II/2017 U1 ('Oumuamua). *The Astrophysical Journal Letters* 850, L38. doi:10.3847/2041-8213/aa9989, arXiv:1711.01344.
- Trilling, D.E., Robinson, T., Roegge, A., Chandler, C.O., Smith, N., Loeffler, M., Trujillo, C., Navarro-Meza, S., Glaspie, L.M., 2017b. Implications for Planetary System Formation from Interstellar Object II/2017 U1 ('Oumuamua). *The Astrophysical Journal Letters* 850, L38. doi:10.3847/2041-8213/aa9989, arXiv:1711.01344.
- Van Rossum, G., 2020. The Python Library Reference, release 3.8.2. Python Software Foundation.
- Vavilov, D.E., Medvedev, Y.D., 2019. Dust bombardment can explain the extremely elongated shape of II/'Oumuamua and the lack of interstellar objects. *Monthly Notices of the Royal Astronomical Society* 484, L75–L78. doi:10.1093/mnras/1/sly244, arXiv:1812.11334.
- Virtanen, P., Gommers, R., Oliphant, T.E., Haberland, M., Reddy, T., Cournapeau, D., Burovski, E., Peterson, P., Weckesser, W., Bright, J., van der Walt, S.J., Brett, M., Wilson, J., Millman, K.J., Mayorov, N., Nelson, A.R.J., Jones, E., Kern, R., Larson, E., Carey, C.J., Polat, I., Feng, Y., Moore, E.W., VanderPlas, J., Laxalde, D., Perktold, J., Cimrman, R., Henriksen, I., Quintero, E.A., Harris, C.R., Archibald, A.M., Ribeiro, A.H., Pedregosa, F., van Mulbregt, P., SciPy 1.0 Contributors, 2020. SciPy 1.0: Fundamental Algorithms for Scientific Computing in Python. *Nature Methods* 17, 261–272. doi:10.1038/s41592-019-0686-2.
- Williams, G.V., 2017. 2017-U181. *Minor Planet Electronic Circulars*.
- Zhou, W.H., 2020. 'Oumuamua's Rotation with the Mechanical Torque Produced by Interstellar Medium. *The Astrophysical Journal* 899, 42. doi:10.3847/1538-4357/ab9f3e, arXiv:1911.12228.